A Direct Domain-Decomposition-Based Time-Domain Finite-Element Method of Linear Complexity for Simulating Multiscaled Structures in Integrated Circuit Systems

Duo Chen and Dan Jiao, *Senior Member, IEEE*

***Abstract*—A direct domain-decomposition-based time-domain finite-element method of linear complexity is developed to overcome the challenge of simulating a wide range of geometrical scales present in an integrated circuit (IC) system. Via a set of orthogonal prism vector basis functions, we decompose the entire 3-D system of an IC problem into 2-D subsystems and then into 1-D subsystems with negligible computational cost. We then further decompose each 1-D subsystem into two domains, one with conductors and the other one with dielectrics. A direct solution without any iteration is proposed to solve the resulting system in linear complexity. Furthermore, the method allows for the use of different meshes in different domains. Numerical simulations of ICs and package problems have demonstrated the accuracy, linear complexity, and meshing flexibility of the proposed method.**

***Index Terms*—Direct solvers, domain decomposition, finite-element methods, multiscale, time-domain electromagnetic analysis, very large scale integrated circuits.**

I. Introduction

The scaling of supply voltages and the increased level of integration have made the analysis and design of microelectronic systems increasingly challenging. To sustain the scaling and integration of digital, analog, mixed-signal, and RF circuits for years to come, an electromagnetic solution is indispensable to overcome the fundamental limits of a circuit-based analysis.

There are two major challenges associated with the electromagnetics-based analysis of very large scale integrated circuits (ICs): exponentially increased problem size and multiscaled structures. In recent years, a lot of work has been done to address the challenge of simulating very large scale circuits in time domain [1]–[10]. The challenge of simulating multiscaled structures in ICs has also been tackled. One of the fundamental schemes addressing the challenge of multiscale simulation is the domain-decomposition technique. Existing domain-decomposition techniques [11]–[16] have been successful in many applications. However, most of them are iterative solutions, the convergence of which is problem dependent [17]. When simulating very large scale ICs, owing to the complexity of the problem, the number of iterations required for convergence is typically not small and, also, grows with the problem size. The performance of an iterative-solution-based domain-decomposition algorithm is further degraded in transient analysis where the right-hand side changes at every time step.

The contribution of this paper is the development of a direct matrix-solution-based domain decomposition of linear complexity for simulating a wide range of geometrical scales present in an IC. In the proposed direct domain-decomposition method, by recognizing the fact that the origin of the multiscales in an IC is the multiple scales of conductors since dielectric regions have a similar scale, we decompose an IC into two domains. One contains all the conductors; the other includes all the dielectrics. The conductor domain is further naturally decomposed into multiple subdomains, each of which consists of a conductor network that is not physically connected with other conductors. An independent meshing is then performed in each subdomain, where a dielectric subdomain is discretized with a coarse mesh, while a conductor subdomain is discretized with a fine mesh to capture the rapid field variation within skin depth inside conductors. The decomposed dielectric and conductor subdomains are then solved separately by developing a direct domain-decomposition method without any iteration. In each subdomain, the system matrix is solved in linear complexity.

To further accelerate the proposed direct domain-decomposition algorithm, instead of directly decomposing the entire 3-D domain into a conductor domain and a dielectric domain, we first decompose the original 3-D system to 1-D subsystems with negligible computational cost via orthogonal prism vector basis functions we recently developed in [9]. We then perform the conductor-dielectric-based domain decomposition in each 1-D subsystem. By doing so, not only the decomposition of the entire computational domain into a conductor domain and a dielectric domain is made much more convenient, but also we further speed up the proposed direct domain-decomposition algorithm. The accuracy, efficiency, and meshing flexibility of the proposed method have been demonstrated by numerical experiments.

Manuscript received August 03, 2011; revised May 15, 2012; accepted July 18, 2012. Date of publication July 25, 2012; date of current version October 26, 2012. This work was supported by a grant from Intel Corporation, a grant from the U.S. Office of Naval Research under Award N00014-10-1-0482, and grants from the National Science Foundation (NSF) under Awards 0747578 and 1065318.

The authors are with the School of Electrical and Computer Engineering, Purdue University, West Lafayette, IN 47907 USA (e-mail: djiao@purdue.edu).

Color versions of one or more of the figures in this paper are available online at http://ieeexplore.ieee.org.

Digital Object Identifier 10.1109/TAP.2012.2210271

II. Time-Domain Finite-Element-Based Electromagnetic Analysis of ICs

The electric field $\mathbf{E}$ inside a 3-D IC satisfies the second-order vector wave equation

$$\nabla \times \left[\mu_r^{-1}\nabla \times \mathbf{E}(\mathbf{r},t)\right] + \mu_0\varepsilon\partial_t^2\mathbf{E}(\mathbf{r},t) + \mu_0\sigma\partial_t\mathbf{E}(\mathbf{r},t) = -\mu_0\partial_t\mathbf{J}(\mathbf{r},t) \quad (1)$$

subject to certain boundary conditions. In (1), $\mathbf{J}$ is current density, $\mathbf{r}$ is a point in 3-D space, t denotes time, μ_r is relative permeability, μ_0 is free-space permeability, ε is permittivity, and σ is conductivity. In IC and package problems, it is very important to account for the conductivity of metals and model fields inside conductors. This is because fields penetrate into conductors due to the small feature sizes of the IC and package structures and also because of their broadband working frequencies that start from direct current (dc).

A time-domain finite-element solution of (1) and its boundary condition results in the following system of ordinary differential equations [18]:

$$\mathbf{T}\frac{d^2\{u\}}{dt^2} + (\mathbf{R}+\mathbf{V})\frac{d\{u\}}{dt} + \mathbf{S}\{u\} + \{f\} = 0 \quad (2)$$

in which $\{u\}$ is the unknown field vector, $\mathbf{T}$, $\mathbf{R}$, $\mathbf{S}$, and $\mathbf{V}$ are square matrices that are assembled from their elemental contributions as the following:

$$\begin{aligned} \mathbf{T}_{ij}^e &= \mu_0\varepsilon\langle \mathbf{N}_i, \mathbf{N}_j\rangle_V \\ \mathbf{R}_{ij}^e &= \mu_0\sigma\langle \mathbf{N}_i, \mathbf{N}_j\rangle_V \\ \mathbf{S}_{ij}^e &= \mu_r^{-1}\langle \nabla\times\mathbf{N}_i, \nabla\times\mathbf{N}_j\rangle_V \\ \mathbf{V}_{ij}^e &= \frac{1}{c}\langle \hat{n}\times\mathbf{N}_i, \hat{n}\times\mathbf{N}_j\rangle_S \end{aligned} \quad (3)$$

while the excitation vector $\{f\}$ in (2) is assembled from

$$f = \mu_0\langle \mathbf{N}_i, \partial_t\mathbf{J}\rangle_V. \quad (4)$$

In (3) and (4), $\mathbf{N}$ is the vector basis function used to expand electric field $\mathbf{E}$ in each element, c is the speed of light, $\hat{n}$ is a unit vector normal to truncation boundary S and pointing outward, $\langle .,.\rangle_S$ denotes a surface integration, and $\langle .,.\rangle_V$ denotes a volume integration. Matrix $\mathbf{V}$ is related to the absorbing boundary condition. If the first-order absorbing boundary condition is employed to truncate the 3-D computational domain, the matrix element of $\mathbf{V}$ is the same as that shown in (3). If other types of absorbing boundary conditions are used, $\mathbf{V}$ can be modified correspondingly.

Matrix $\mathbf{T}$ is associated with displacement current, while $\mathbf{R}$ is associated with conduction current. It is well known that *inside* a conductor, the conduction current is dominant because the magnitude of the displacement current is orders of magnitude smaller than that of the conduction current from dc to very high frequencies. Therefore, inside conductors, the term associated with displacement current, which is the $\mathbf{T}$-related term, can be neglected, and hence (2) becomes

$$\mathbf{R}\frac{d\{u\}}{dt} + \mathbf{S}\{u\} + \{f'\} = 0 \quad (5)$$

where f' denotes the excitation from both the current source and the coupling from the dielectric region to the conductor region. Equation (5) is a first-order ordinary differential equation in time domain. Its solution has an analytical time dependence, which can be obtained efficiently using the scheme shown in [10]. The resultant scheme is also unconditionally stable because it allows for the use of any large time step without violating stability in time-domain simulation. Moreover, (5) can also be simulated by a forward difference scheme that permits the use of a very large time step, which will be shown in Section III-E.

III. Proposed Direct Domain-Decomposition Method of Linear Complexity

A. Direct Domain Decomposition for Separating the Solution in Conductor Domain From That in Dielectric Domain for Efficient Simulation of Multiscaled Structures

1) Decompose the System Into a Conductor Domain and a Dielectric Domain: In an IC system, there exists a wide range of geometrical scales. For example, a metallic wire in on-chip metal 2 (M2) layer can be less than 0.5 μm in width, while a package plane can be as wide as a few millimeters. Despite the wide range of geometrical scales, the conductors are the ones that have multiple scales; the dielectric materials all have a similar scale. By recognizing this fact, we propose to decompose an IC problem into two subdomains. One contains all the conductors; the other includes all the dielectrics. The conductor domain again can be naturally decomposed into multiple subdomains that are fully decoupled, each of which consists of a conductor network that is not physically connected with other conductors. For example, in a 3-D bus structure, each single bus makes a subdomain that is decoupled from other subdomains because it is physically disconnected with other buses.

There are a number of advantages of decomposing an IC problem into a conductor domain and a dielectric domain. First, the multiple scales present in an IC system can be divided into different subdomains to conquer, with each subdomain having its own scale. For example, the subdomain formed by a bus in an M2 layer has a very small feature size, while the subdomain formed by a package plane has a very large scale. Since the matrix blocks corresponding to physically disconnected conductor subdomains are naturally decoupled from each other, these matrix blocks can be solved independently. Hence, one does not need to tackle the orders-of-magnitude different scales simultaneously. Second, each subdomain can be meshed independently based on its own geometrical scale and physical property, hence providing flexibility in meshing and efficiency in computation. For example, the dielectric domain that has a very slow field variation in space can be discretized with a coarse mesh, whereas the conductor domain that has a very rapid field variation within skin depth can be discretized with a fine mesh. In addition, the conductors in different metal layers can be discretized with different mesh density. Hence, the total number of unknowns can be reduced, which helps speed up the simulation. Third, the conductor domain is governed by the diffusion equation while the dielectric domain is governed by the wave equation. By separating these two domains from each other, one

can take advantage of the different physics in different domains to solve a different set of equations in each domain to speed up the simulation.

Although the matrix block in each conductor subdomain is decoupled from that in the other conductor subdomains, the matrix block corresponding to the dielectric domain is coupled to all the conductor subdomains, which makes an efficient domain-decomposition difficult. Most of the existing domain decomposition algorithms rely on iterative solvers to handle the coupling between different subdomains, the convergence of which is problem dependent. In Sections III-A2 and III-A3, we show how to efficiently simulate the system of equations in the conductor domain and that in the dielectric domain, from which a direct domain-decomposition algorithm is developed without the need of any iteration. In Section III-B and Section III-C, we propose a linear-complexity implementation of the proposed direct domain-decomposition algorithm, and hence achieving optimal complexity.

2) Time-Domain Discretization of the System Equations in Different Domains: The 3-D computational domain of an IC problem is decomposed into two subdomains: conductor domain and dielectric domain. Correspondingly, we cast the original system of (2) into the following form:

$$\begin{bmatrix} \mathbf{T}_{ii} & \mathbf{T}_{io} \\ \mathbf{T}_{oi} & \mathbf{T}_{oo} \end{bmatrix} \frac{d^2}{dt^2} \begin{Bmatrix} u_i \\ u_o \end{Bmatrix} + \begin{bmatrix} \mathbf{R}_{ii} & 0 \\ 0 & \mathbf{V}_{oo} \end{bmatrix} \frac{d}{dt} \begin{Bmatrix} u_i \\ u_o \end{Bmatrix} + \begin{bmatrix} \mathbf{S}_{ii} & \mathbf{S}_{io} \\ \mathbf{S}_{oi} & \mathbf{S}_{oo} \end{bmatrix} \begin{Bmatrix} u_i \\ u_o \end{Bmatrix} = \begin{Bmatrix} 0 \\ -f_o \end{Bmatrix} \quad (6)$$

where u_i denotes all the unknowns inside conductors as well as those on the conducting surface and u_o denotes those outside conductors. It is worth mentioning that we do not separately formulate a boundary value problem for the conductor domain and the dielectric domain. Instead, a single boundary value problem is formulated for the entire computational domain, yielding the linear system of equations shown in (2). Equation (6) is simply another representation of (2), in which the unknowns are categorized into two groups: u_i and u_o. Since in a finite-element method the current source excitation is usually launched from the region outside conductors, the excitation of the first row in (6) is zero. Since the unknowns residing on the conductor surface are categorized into u_i, the matrix $\mathbf{R}$ is only nonzero in the ii-block. The $\mathbf{V}_{ii}$ is not considered in (6) because it is negligible compared to $\mathbf{R}_{ii}$.

The dielectric domain is governed by the second row of equations in (6), which can be written as

$$\mathbf{T}_{oo}\frac{d^2\{u_o\}}{dt^2} + \mathbf{V}_{oo}\frac{d\{u_o\}}{dt} + \mathbf{S}_{oo}\{u_o\} = -\mathbf{T}_{oi}\frac{d^2\{u_i\}}{dt^2} - \mathbf{S}_{oi}\{u_i\} - \{f_o\}. \quad (7)$$

By adopting a central difference scheme to approximate the first- and second-order time derivatives in (7), we obtain

$$\begin{aligned}(\mathbf{T}_{oo} + 0.5\Delta t\mathbf{V}_{oo})\{u_o\}^{n+1} + \mathbf{T}_{oi}\{u_i\}^{n+1} \\ = (2\mathbf{T}_{oo} - \Delta t^2\mathbf{S}_{oo})\{u_o\}^n + (2\mathbf{T}_{oi} - \Delta t^2\mathbf{S}_{oi})\{u_i\}^n \\ + [0.5\Delta t\mathbf{V}_{oo} - \mathbf{T}_{oo}]\{u_o\}^{n-1} - \mathbf{T}_{oi}\{u_i\}^{n-1} - \Delta t^2\{f_o\}^n\end{aligned} \quad (8)$$

where Δt represents the time step.

The conductor domain is characterized by the first row of equations in (6). Inside a conductor, the displacement current is orders of magnitude smaller than that of the conduction current from dc to very high frequencies. Hence, the $\mathbf{T}_{ii}$ can be ignored in the first row of (6). Thus, we have

$$\mathbf{R}_{ii}\frac{d\{u_i\}}{dt} + \mathbf{S}_{ii}\{u_i\} = -\mathbf{T}_{io}\frac{d^2\{u_o\}}{dt^2} - \mathbf{S}_{io}\{u_o\}. \quad (9)$$

It is known that a central difference scheme cannot guarantee stability in the time-domain simulation of a diffusion equation. Here, we adopt a forward difference scheme to approximate the first-order time derivative of the u_i with respect to time. We obtain

$$\begin{aligned}\Delta t\mathbf{R}_{ii}\{u_i\}^{n+1} + \mathbf{T}_{io}\{u_o\}^{n+1} \\ = \Delta t(\mathbf{R}_{ii} - \Delta t\mathbf{S}_{ii})\{u_i\}^n + (2\mathbf{T}_{io} - \Delta t^2\mathbf{S}_{io})\{u_o\}^n \\ - \mathbf{T}_{io}\{u_o\}^{n-1}.\end{aligned} \quad (10)$$

Combining (8) and (10), the system of equations for the entire domain including both dielectric and conductor subdomains becomes

$$\begin{aligned}\begin{bmatrix} \Delta t\mathbf{R}_{ii} & \mathbf{T}_{io} \\ \mathbf{T}_{oi} & \mathbf{T}_{oo} + 0.5\Delta t\mathbf{V}_{oo} \end{bmatrix} \begin{Bmatrix} u_i \\ u_o \end{Bmatrix}^{n+1} \\ = \begin{bmatrix} \Delta t(\mathbf{R}_{ii} - \Delta t\mathbf{S}_{ii}) & 2\mathbf{T}_{io} - \Delta t^2\mathbf{S}_{io} \\ 2\mathbf{T}_{oi} - \Delta t^2\mathbf{S}_{oi} & 2\mathbf{T}_{oo} - \Delta t^2\mathbf{S}_{oo} \end{bmatrix} \begin{Bmatrix} u_i \\ u_o \end{Bmatrix}^n \\ + \begin{bmatrix} \mathbf{0} & -\mathbf{T}_{io} \\ -\mathbf{T}_{oi} & 0.5\Delta t\mathbf{V}_{oo} - \mathbf{T}_{oo} \end{bmatrix} \begin{Bmatrix} u_i \\ u_o \end{Bmatrix}^{n-1} \\ + \begin{Bmatrix} 0 \\ -\Delta t^2 f_o \end{Bmatrix}^n.\end{aligned} \quad (11)$$

The above is solved at each instant to obtain field solutions. Clearly, the computational bottleneck is the solution of the left-hand-side matrix. In Section III-A3, we show how to perform a direct domain decomposition to solve (11) without invoking iterations.

3) Direct Domain-Decomposition Method: To help explain the proposed direct domain-decomposition algorithm, we rewrite (11) in a compact form as follows:

$$\begin{bmatrix} \mathbf{A}_{ii} & \mathbf{A}_{io} \\ \mathbf{A}_{oi} & \mathbf{A}_{oo} \end{bmatrix} \begin{Bmatrix} u_i \\ u_o \end{Bmatrix} = \begin{Bmatrix} b_i \\ b_o \end{Bmatrix} \quad (12)$$

where

$$\begin{aligned}\mathbf{A}_{ii} &= \Delta t\mathbf{R}_{ii} \\ \mathbf{A}_{io} &= \mathbf{T}_{io} = \mathbf{A}_{oi}^T \\ \mathbf{A}_{oo} &= \mathbf{T}_{oo} + 0.5\Delta t\mathbf{V}_{oo}\end{aligned} \quad (13)$$

the $\mathbf{A}_{io}$ and $\mathbf{A}_{oi}$ represent the interaction between the unknowns on the conductor surface and the unknowns in dielectric domain, and $\{b_i, b_o\}^T$ denotes the right-hand side of (11). As can be seen from (11), the right-hand side changes at every time step.

In Fig. 1, the dielectric domain is denoted by oo-domain, and the conductor domain is denoted by the ii-domain. To describe the proposed domain-decomposition algorithm more clearly, we define the area in the oo-domain, which contains all the unknowns that interact with the ii-domain, as the buffer region,

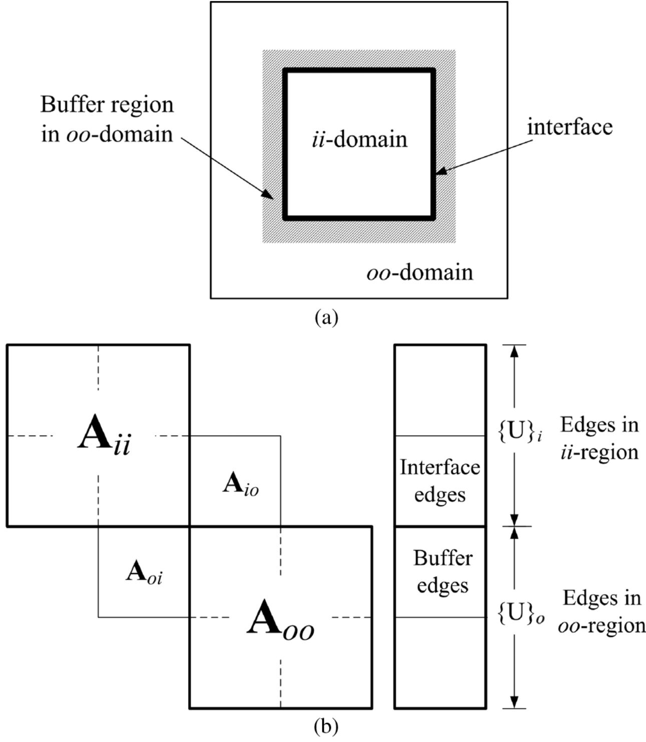

Fig. 1. (a) Illustration of the conductor domain (ii-domain) and dielectric domain (oo-domain), interface, and buffer regions. (b) Relationship between $\mathbf{A}_{ii}$, $\mathbf{A}_{io}$, $\mathbf{A}_{oi}$, and $\mathbf{A}_{oo}$.

which is the gray region shown in Fig. 1(a). In an edge-based finite-element method, the degrees of freedom are assigned to edges. We call the edges located in the buffer region as buffer edges, and the edges on the conductor surface as interface edges. The relationship between the matrix blocks in (12) is illustrated in Fig. 1(b).

To solve (12) directly, we first reduce the whole system to that in the conductor domain via Schur complement, thus obtaining

$$\left[\mathbf{A}_{ii} - \mathbf{A}_{io}\mathbf{A}_{oo}^{-1}\mathbf{A}_{oi}\right]\{u_i\} = \{b_i\} - \mathbf{A}_{io}\mathbf{A}_{oo}^{-1}\{b_o\}. \quad (14)$$

By solving (14), we obtain the solution of $\{u_i\}$, from which we can retrieve the solution of $\{u_o\}$ by

$$\mathbf{A}_{oo}\{u_o\} = \{b_o\} - \mathbf{A}_{oi}\{u_i\}. \quad (15)$$

The Schur complement $[\mathbf{A}_{ii} - \mathbf{A}_{io}\mathbf{A}_{oo}^{-1}\mathbf{A}_{oi}]$ in (14) carries the contribution from the oo-domain to the ii-domain. Its direct solution is generally regarded computationally expensive since the original matrix structure of $\mathbf{A}_{ii}$ is altered significantly by $\mathbf{A}_{io}\mathbf{A}_{oo}^{-1}\mathbf{A}_{oi}$, and also the resultant matrix becomes dense. Therefore, (14) is often solved by iterative solvers in domain-decomposition methods. In the following, we show that (14) concerned in this work can be solved directly without any iteration by using the solution of $\mathbf{A}_{ii}$ and the solution of $\mathbf{A}_{oo}$ only.

Based on the expressions of $\mathbf{T}$ and $\mathbf{R}$ shown in (3), we have the following relationship:

$$\frac{\mathbf{R}_{i,j}}{\mathbf{T}_{i,j}} \sim \frac{\sigma}{\varepsilon} \to 10^{18} \quad (16)$$

since the metal conductivity is in the order of 10^7. This indicates that the elements in $\mathbf{T}$ and $\mathbf{R}$ are orders of magnitude different. From (16) and (13), we can see that the magnitudes of $\mathbf{A}_{ii}$'s elements and those of $\mathbf{A}_{io}\mathbf{A}_{oo}^{-1}\mathbf{A}_{oi}$'s elements are also very different. The $\mathbf{A}_{ii}$ is $\Delta t\mathbf{R}_{ii}$, while $\mathbf{A}_{oo}$ can be estimated as $\mathbf{T}_{oo}$, since the $\mathbf{V}$-related term is significantly smaller than the $\mathbf{T}$-based term. Thus, the norm of $\mathbf{A}_{io}\mathbf{A}_{oo}^{-1}\mathbf{A}_{oi}$ over that of $\mathbf{A}_{ii}$ can be evaluated as

$$\frac{\left\|\mathbf{A}_{io}\mathbf{A}_{oo}^{-1}\mathbf{A}_{oi}\right\|}{\|\mathbf{A}_{ii}\|} \approx \frac{\left\|\mathbf{T}_{io}\mathbf{T}_{oo}^{-1}\mathbf{T}_{oi}\right\|}{\Delta t\|\mathbf{R}_{ii}\|} \le \frac{\|\mathbf{T}_{io}\|\left\|\mathbf{T}_{oo}^{-1}\right\|\|\mathbf{T}_{oi}\|}{\Delta t\|\mathbf{R}_{ii}\|}.$$

Since $\mathbf{T}_{oo}$ is a Hermitian matrix, it is unitarily diagonalizable. Thus, we have

$$\mathbf{T}_{oo} = \mathbf{QDQ}^{-1}$$

where $\mathbf{Q}$ is a unitary matrix, and $\mathbf{D}$ is a diagonal eigenvalue matrix. As a result, we obtain

$$\mathbf{T}_{oo}^{-1} = \mathbf{QD}^{-1}\mathbf{Q}^{-1}$$

and, hence

$$\left\|\mathbf{T}_{oo}^{-1}\right\| = \|\mathbf{D}^{-1}\| = \frac{1}{D_{\min}}$$

where $D_{\min}$, i.e., the minimum value in $\mathbf{D}$, is the minimum eigenvalue of $\mathbf{T}_{oo}$. Thus, we obtain

$$\frac{\left\|\mathbf{A}_{io}\mathbf{A}_{oo}^{-1}\mathbf{A}_{oi}\right\|}{\|\mathbf{A}_{ii}\|} \le \frac{\|\mathbf{T}_{io}\|\|\mathbf{T}_{oi}\|}{\Delta t\|\mathbf{R}_{ii}\|D_{\min}}.$$

Since $\|\mathbf{T}_{oo}\| = \|\mathbf{D}\| = D_{\max}$, the $D_{\min}$ can be estimated from $\|\mathbf{T}_{oo}\|$. As for $\|\mathbf{T}_{io}\|$, $\|\mathbf{T}_{oi}\|$, and $\|\mathbf{R}_{ii}\|$, they can be quantitatively assessed from (3). As a result, we obtain the following estimation:

$$\frac{\left\|\mathbf{A}_{io}\mathbf{A}_{oo}^{-1}\mathbf{A}_{oi}\right\|}{\|\mathbf{A}_{ii}\|} \sim O\left(\frac{\varepsilon}{\Delta t\sigma}\right). \quad (17)$$

For the simulation of ICs and packages, the time step is generally greater than 10^{-16} s. This is because this time step is small enough to capture all of the frequencies that can exist in a circuit response; it is also small enough to maintain the time-domain stability in conditionally stable schemes such as central-difference-based explicit time-domain methods. As a result, (17) is less than 0.01. Hence, $\mathbf{A}_{io}\mathbf{A}_{oo}^{-1}\mathbf{A}_{oi}$ is negligible compared to $\mathbf{A}_{ii}$. Therefore, the computation of (14) becomes the computation of

$$\mathbf{A}_{ii}\{u_i\} = \{b_i\} - \mathbf{A}_{io}\mathbf{A}_{oo}^{-1}\{b_o\}. \quad (18)$$

If a rigorous solution is pursued and no approximation is allowed, the solution of (14) can be computed using the following Neumann series:

$$\left[\mathbf{A}_{ii} - \mathbf{A}_{io}\mathbf{A}_{oo}^{-1}\mathbf{A}_{oi}\right]^{-1} = \left[\mathbf{I} + \mathbf{A}_{ii}^{-1}\mathbf{A}_{io}\mathbf{A}_{oo}^{-1}\mathbf{A}_{oi} + \left(\mathbf{A}_{ii}^{-1}\mathbf{A}_{io}\mathbf{A}_{oo}^{-1}\mathbf{A}_{oi}\right)^2 + \dots\right]\mathbf{A}_{ii}^{-1} \quad (19)$$

which can converge within a few terms since the norm of $\mathbf{A}_{ii}^{-1}\mathbf{A}_{io}\mathbf{A}_{oo}^{-1}\mathbf{A}_{oi}$ is much less than 1. From (19), it can be seen that even though a rigorous solution is pursued, the solution of Schur complement can be found by computing $\mathbf{A}_{ii}^{-1}$ and $\mathbf{A}_{oo}^{-1}$, and hence from the solution of $\mathbf{A}_{ii}$ and $\mathbf{A}_{oo}$ only. As a result, we achieve a direct domain decomposition without any iteration. The matrix solution in the ii-domain is completely decoupled from that in the oo-domain. Moreover, independent meshing can be performed in two domains.

B. Direct Domain Decomposition for Decomposing a 3-D System Into 1-D Subsystems, With Each 1-D Subsystem Further Decomposed Into Conductor and Dielectric Subsystems

As can be seen from Section III-A, we solve two decomposed subsystems (18) [or (19)] and (15) to obtain the solution of the original problem. It is clear that with the proposed direct decomposition algorithm, the solutions of $\mathbf{A}_{ii}$ and $\mathbf{A}_{oo}$ are fully decoupled. To further accelerate the proposed direct domain-decomposition algorithm, instead of directly decomposing the entire 3-D domain into a conductor domain and a dielectric domain, we will first decompose the original 3-D system to 1-D subsystems with negligible computational cost. We then perform the conductor-dielectric decomposition in each 1-D subsystem. By doing so, not only the decomposition of the entire computational domain into a conductor domain and a dielectric domain is made much more convenient, but also we further speed up the proposed direct domain-decomposition algorithm. The details of this step are given as follows.

We discretize the computational domain into triangular prism elements. For ICs and package problems, triangular prism elements are indeed natural for choice. Even if one discretizes the structure using tetrahedral elements, layers of tetrahedral elements will be obtained since the structure is layered in nature. For a Manhattan-type IC that is most widely used today, the structure is layered in any direction (in other words, the geometry can be sliced into layers while the material is not required to be layered). Furthermore, if one can accept a staircase approximation in geometrical modeling along one direction, a triangular prism element can be used to discretize arbitrarily shaped 3-D structures. In any case, it provides a better geometrical modeling capability than what a grid can offer.

In each triangular prism element, we expand the unknown electric field $\mathbf{E}$ into orthogonal prism vector basis functions developed in [9], which are illustrated in Fig. 2. In these basis functions, the set of bases that are associated with upper and lower planes of the prism, i.e., bases $\mathbf{N}_1-\mathbf{N}_6, \mathbf{N}_{10}-\mathbf{N}_{15}$, are called surface basis functions while those associated with vertical edges are called volume basis functions (i.e., $\mathbf{N}_7-\mathbf{N}_9$). These bases have two important properties. First, surface basis functions and volume basis functions are perpendicular to each other because of the geometrical nature of a prism element, as shown in Fig. 2. Second, on each surface, the surface basis functions are orthogonal to each other because of the property of the orthogonal vector bases.

With the first property, without any computational cost, we can decompose the original 3-D system of any IC problem into

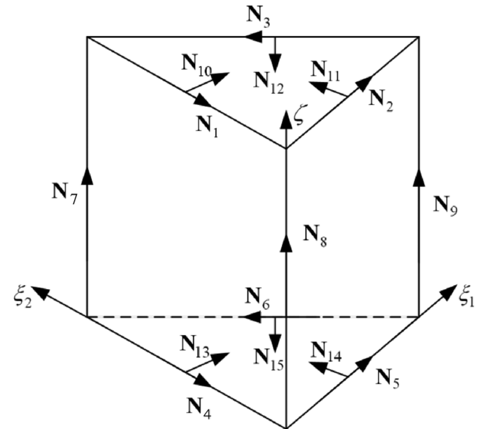

Fig. 2. Illustration of the orthogonal prism vector basis functions (after [9]).

two 2-D subsystems, i.e., surface unknown system and volume unknown system, as shown in the following:

$$\begin{aligned}\mathbf{P}_S x_S &= b_S \\ \mathbf{P}_{Vl} x_{Vl} &= b_{Vl}, \qquad l=1,2,\ldots,L\end{aligned} \tag{20}$$

in which $\mathbf{P}_S$ denotes the surface unknown system, the volume unknown system consists of decoupled subsystems in each layer, $\mathbf{P}_{Vl}$ $(l=1,2,\ldots,L)$, x_S and x_V denote the surface unknowns, and volume unknowns, respectively, while b_S and b_{Vl} denote the right-hand side of (11) corresponding to the surface and volume unknowns, respectively.

With the second property, we can further decompose the 2-D surface unknown system $\mathbf{P}_S$ into 1-D subsystems. The 2-D surface unknown system $\mathbf{P}_S$ is composed of $\mathbf{D}_l$ and $\mathbf{\Lambda}_l$ $(l=1,2,\ldots,L)$ blocks, as shown in Fig. 3. Each of $\mathbf{D}_l$ and $\mathbf{\Lambda}_l$ is diagonal due to the orthogonality of the vector basis functions [9]. We assume that the discretization results in $N_{\rm s}$ unknowns on a single surface and L layers, and hence $L+1$ surfaces. By permuting unknowns, the $\mathbf{P}_S$ shown in Fig. 3 can be naturally transformed to a block diagonal matrix of $N_{\rm s}$ blocks, as shown in the following:

$$\mathbf{P}_S = \begin{bmatrix} \tilde{\mathbf{T}}_1 & & & \\ & \tilde{\mathbf{T}}_2 & & \\ & & \cdots & \\ & & & \tilde{\mathbf{T}}_{N_S} \end{bmatrix}. \tag{21}$$

More important, each diagonal block $\tilde{\mathbf{T}}_i$ $(i=1,2,\ldots,N_s)$ is a tridiagonal matrix of size $L+1$

$$\tilde{\mathbf{T}}_i = \begin{bmatrix} \mathbf{D}_{1,i} & \mathbf{\Lambda}_{1,i} & & \\ \mathbf{\Lambda}_{1,i} & \mathbf{D}_{1,i}+\mathbf{D}_{2,i} & \mathbf{\Lambda}_{2,i} & \\ & & \cdots & \mathbf{\Lambda}_{L,i} \\ & & \mathbf{\Lambda}_{L,i} & \mathbf{D}_{L+1,i} \end{bmatrix} \tag{22}$$

where $\mathbf{D}_{j,i}$ and $\mathbf{\Lambda}_{j,i}$ denote the ith entries in matrices $\mathbf{D}_j$ and $\mathbf{\Lambda}_j$, respectively. Essentially, matrix $\mathbf{P}_S$ in (21) is decomposed into multiple 1-D susbsystems $\tilde{\mathbf{T}}_i$. Each 1-D subsystem is associated with one surface basis function and its counterparts along the prism (layer) growth direction. Again, the decomposition

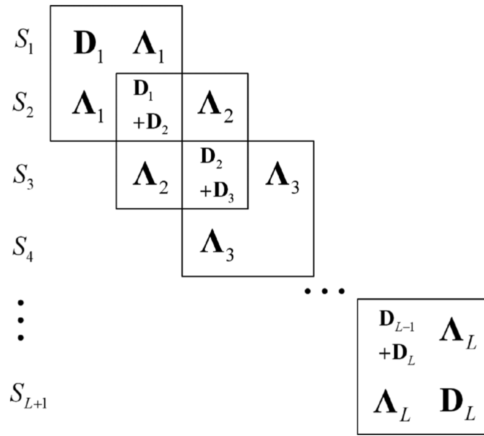

Fig. 3. Illustration of the surface unknown system $\mathbf{P}_S$.

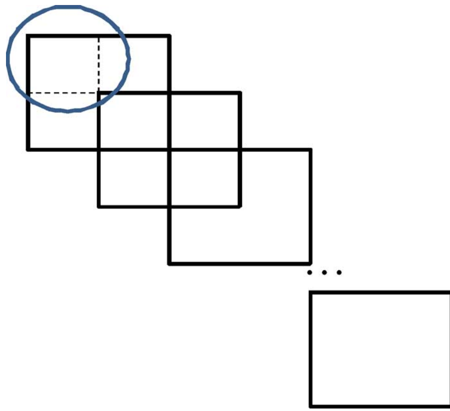

Fig. 4. Illustration of $\mathbf{P}_{Vl}$, a volume unknown subsystem in each layer.

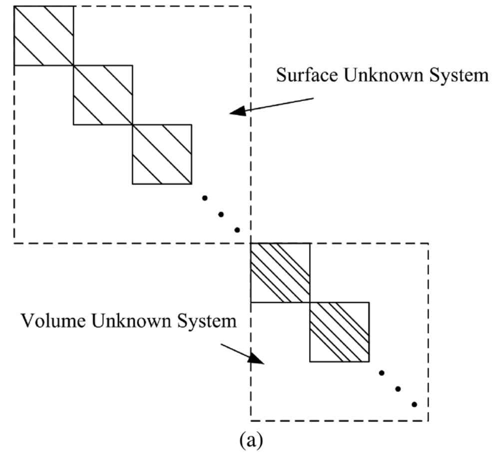

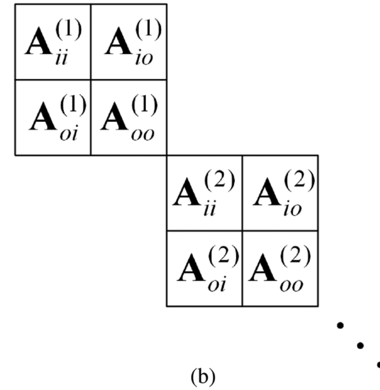

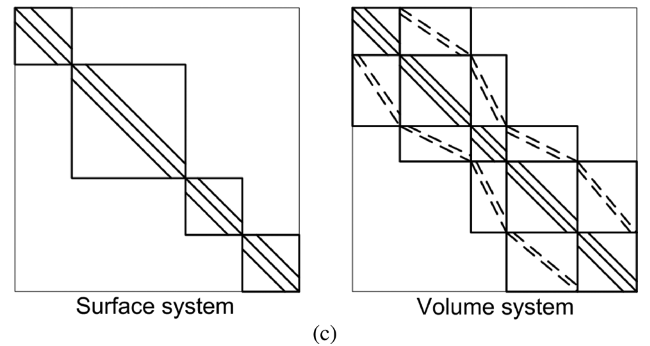

Fig. 5. (a) Matrix structure of the decomposed system made of 1-D blocks. (b) Illustration of the further decomposition into ii- and oo-subsystems in each 1-D block. (c) Structure of $\mathbf{A}_{ii}$ or $\mathbf{A}_{oo}$ in a surface-based 1-D subsystem and a volume-based subsystem.

from a 2-D surface unknown system to 1-D subsystems shown in (21) is done without any computational cost.

As for the volume-unknown-based subsystem $\mathbf{P}_{Vl}$ in each layer, it is a block tridiagonal matrix, as shown in Fig. 4. Each block of $\mathbf{P}_{Vl}$, the size of which is highlighted by the circle shown in Fig. 4, represents a 1-D subsystem whose dimension is the number of dielectric stacks in an IC, a constant that does not grow with problem size.

The final matrix structure resulting from the aforementioned decomposition from a 3-D system to 1-D subsystems is shown in Fig. 5(a), which is a block diagonal matrix. Each diagonal block in the surface unknown system represents a 1-D subsystem corresponding to $\tilde{\mathbf{T}}_i$, shown in (22), the dimension of which is the number of layers. Each diagonal block in the volume unknown system represents a 2-D subsystem in each layer, the detailed structure of which is shown in Fig. 4. The 2-D subsystem in each layer is made of 1-D blocks whose dimension is the number of dielectric stacks.

Next, in each diagonal block shown in Fig. 5(a), we decompose the unknowns into i- and o-unknowns, where i denotes a conductor domain, and o denotes a dielectric domain. By doing so, the conductor-dielectric decomposition is made very convenient. The final decomposed system has a matrix structure shown in Fig. 5(b). Each combined $o-i$ system is then solved by the direct domain-decomposition algorithm described in Section III-A. The rows of equations in each 1-D subsystem corresponding to i-unknowns are shown in (18), while the rows of equations corresponding to o-unknowns are shown in (15).

C. Linear-Complexity Direct Solution

In the decomposed system shown in Fig. 5(a), each 1-D surface unknown subsystem, which is $\tilde{\mathbf{T}}_i$, shown in (22), is a tridiagonal matrix, and each single-layer volume unknown subsystem $\mathbf{P}_{Vl}$ is a block tridiagonal matrix shown in Fig. 4, with each block having a 1-D size.

After the $ii-oo$ decomposition illustrated in Fig. 5(b), the matrix property of the resultant $\mathbf{A}_{ii}$ and $\mathbf{A}_{oo}$ in each subsystem remains the same. In surface unknown system, $\mathbf{A}_{ii}$ and $\mathbf{A}_{oo}$ are block diagonal matrices, with each block being tridiagonal, as shown in the left figure of Fig. 5(c). Therefore, the direct solution of $\mathbf{A}_{ii}$ and $\mathbf{A}_{oo}$ in the surface unknown based system

has a linear complexity due to the tridiagonal matrix structure [19]. Similarly, for each subsystem that is formed by volume unknowns in a single layer, with the original structure shown in Fig. 4, which is a block tridiagonal matrix, the resultant $\mathbf{A}_{ii}$ and $\mathbf{A}_{oo}$ remain to be block tridiagonal matrices, as shown in the right figure of Fig. 5(c). In this figure, the dashed lines in the off-diagonal blocks indicate that some of the nonzero entries in the original volume unknown system in Fig. 5(a) have been categorized into $\mathbf{A}_{io}$ and $\mathbf{A}_{oi}$ blocks, hence those elements become zero in $\mathbf{A}_{ii}$ and $\mathbf{A}_{oo}$. However, these zero elements do not affect the matrix structure. The matrix remains to be a block tridiagonal matrix. In [9], the underlying volume unknown solver is an iterative solver. Although the iteration number is not large, the performance of an iterative solver deteriorates when the number of right-hand sides is large, which is typically true in a time-domain solver. To address this problem, in this work, we solve the block tridiagonal matrix by using block UV factorization [19] or block reduction recovery method [9] in linear complexity, based on the fact that the block size is a constant since the dimension of each block in a single-layered volume unknown system is equal to the number of dielectric stacks in an IC. Assuming the number of stacks is N_x and the number of blocks in a volume unknown subsystem is M, the overall complexity of a block UV-based direct solution is $O(N_x^2 M)$. Since $N_x M = M_v$, where M_V is the total number of volume unknowns in a single layer, the complexity is $O(N_x M_V)$. Since N_x is a constant, the complexity is linear. With $\mathbf{A}_{ii}$ and $\mathbf{A}_{oo}$ in both surface unknown system and volume unknown system solved in linear complexity, the entire solution of the proposed direct domain-decomposition method has a linear complexity.

D. Nonconformal Mesh

Since $\mathbf{A}_{ii}$ and $\mathbf{A}_{oo}$ are fully decoupled in the final system, we can mesh the conductor domain and the dielectric domain independently. To capture the rapid field variation inside conductors, we use a fine mesh to discretize the ii-domain (conductor domain). In the oo-domain (dielectric domain), we use a coarse mesh. The resulting system with a nonconformal mesh is computed as follows:

$$\mathbf{A}_{ii}\{u_i\} = \{b_i\} - \mathbf{A}_{io}\left(\mathbf{P}_{io}\left(\mathbf{A}_{oo}^{-1}\{b_o\}\right)\right) \quad (23)$$

$$\mathbf{A}_{oo}\{u_o\} = \{b_o\} - \mathbf{A}_{oi}\left(\mathbf{P}_{oi}\{u_i\}\right) \quad (24)$$

in which $\mathbf{P}_{io}$ is a projection matrix that projects the field solution from the oo-domain with a coarse mesh to the ii-domain with a fine mesh, while $\mathbf{P}_{oi}$ projects the field solution on interface edges from ii-domain with a fine mesh to oo-domain with a coarse mesh. They both are extremely sparse matrices. In (23), $\mathbf{A}_{oo}^{-1}\{b_o\}$ denotes a field solution in the oo-domain that has a coarse mesh, while $\mathbf{A}_{io}$ is constructed based on the fine mesh. In $\mathbf{A}_{io}$, only the rows corresponding to the interface edges are nonzero, as illustrated in Fig. 1(b). Each nonzero entry in $\mathbf{A}_{io}$ denotes the interaction between an interface edge and a buffer edge. Therefore, the vector that $\mathbf{A}_{io}$ multiplies with is the field solution in the buffer region. Hence, the role that $\mathbf{P}_{io}$ plays is to interpolate the field solution $\mathbf{A}_{oo}^{-1}\{b_o\}$, which is obtained in a coarse mesh, thus obtaining the field solution in the buffer region that has a fine mesh. Consider an arbitrary edge j in the buffer region. Assume that it is located in the kth triangular prism element in the oo-domain. The jth row of $\mathbf{P}_{io}(\mathbf{A}_{oo}^{-1}\{b_o\})$, which is the field solution at buffer edge j, can be evaluated as follows:

$$\left[\mathbf{P}_{io}\left(\mathbf{A}_{oo}^{-1}\{b_o\}\right)\right]_j = \mathbf{E}(x_j, y_j, z_j)\cdot\hat{t}_j = \left(\sum_{m=1}^{15} u_m^{(o)}\mathbf{N}_m^k(x_j, y_j, z_j)\right)\cdot\hat{t}_j \quad (25)$$

where (x_j, y_j, z_j) is the center point of the buffer edge j, and $\hat{t}_j$ is a unit vector tangential to this buffer edge, $\mathbf{N}_m^k$ $(m = 1, 2, \ldots, 15)$ denotes the orthogonal prism vector basis in the kth element, and $u_m^{(o)}$ is the field solution in the oo-domain provided by $\mathbf{A}_{oo}^{-1}\{b_o\}$. From (25), it can be seen that the elements of $\mathbf{P}_{io}$ can be written as

$$(\mathbf{P}_{io})_{j,e(k,m)} = \mathbf{N}_m^k(x_j, y_j, z_j)\cdot\hat{t}_j \quad (26)$$

where $e(k,m)$ denotes the global edge number of the mth edge in the kth element in the oo-domain.

In (24), $\mathbf{A}_{oi}$ is constructed based on a coarse mesh. It needs to be multiplied by the field solution at the interface edges in the coarse mesh. What $\mathbf{P}_{oi}$ does is to interpolate the field solution u_i at the interface edges in the fine mesh (used for discretizing the conductor domain) to obtain the field solution at the interface edges in the coarse mesh (used in the dielectric domain). It can be constructed in the same way as $\mathbf{P}_{io}$ is constructed. Both $\mathbf{P}_{io}$ and $\mathbf{P}_{oi}$ are extremely sparse matrices, since the interface edges and the buffer edges only account for a very small portion of the entire edges. Thus, the computation of $\mathbf{P}_{io}$- and $\mathbf{P}_{oi}$-based matrix–vector multiplications has a linear complexity and the cost is also negligible.

E. Stability Analysis

Since there are two different time marching schemes in the final system shown in (11), i.e., forward difference for conductor domain and central difference for dielectric domain, we need to perform a stability analysis for each domain. The final stability criterion for the whole system is determined by the minimum time step permitted by each domain.

In the dielectric domain, since a central difference is used, the time step needs to satisfy the following stability criterion [21]:

$$\Delta t_{oo} \leq 2\Big/\sqrt{\rho\left(\mathbf{T}_{oo}^{-1}\mathbf{S}_{oo}\right)} \quad \text{in dielectric domain} \quad (27)$$

in which $\rho(*)$ denotes the spectral radius. In conductor domain, a forward difference is used, the stability of which can be analyzed as follows.

We set the right-hand side of (9) to be zero and perform a z-transform. We obtain

$$\frac{(1-z)}{\Delta t}\{\widehat{u}\} = \mathbf{R}_{ii}^{-1}\mathbf{S}_{ii}\{\widehat{u}\} \quad (28)$$

in which $\{\widehat{u}\}$ denote the z-transform of $\{u\}$. We denote $(1-z)$ by λ. Clearly, $\lambda/\Delta t$ is the eigenvalue of matrix $\mathbf{R}_{ii}^{-1}\mathbf{S}_{ii}$. To make the system stable, we have to bound the magnitude of z to be less than one or inside a unit circle on the complex plane. From $|z| \leq 1$ and $\lambda = (1-z)$, and utilizing the fact that λ is nonnegative real number because $\mathbf{R}_{ii}$ is positive definite and

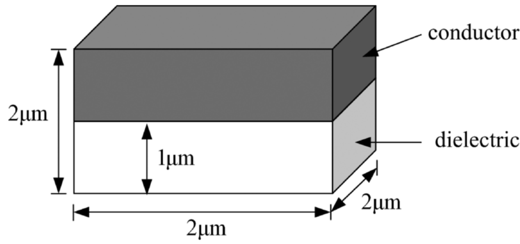

Fig. 6. A cube that is partially filled with copper.

TABLE I
RELATIVE ERROR VERSUS TIME STEP AND NUMBER OF TERMS

Time Step (s)	Error with 1 Term shown in (31)	Error with 2 Terms	Error with 3 Terms
1.0e-13	4.9536e-07	4.7009e-13	2.0258e-19
1.0e-14	4.9536e-06	4.7028e-11	7.2788e-16
1.0e-15	4.9541e-05	4.7031e-09	4.5074e-13
1.0e-16	4.9583e-04	4.7072e-07	4.5114e-10
1.0e-17	5.0010e-03	4.7482e-05	4.5508e-07

$\mathbf{S}_{ii}$ is semipositive definite, we obtain $\lambda_{\max} \leq 2$, where $\lambda_{\max}$ is the largest value of λ, which is $\Delta t \rho(\mathbf{R}_{ii}^{-1}\mathbf{S}_{ii})$. Therefore, the stability criterion for the conductor domain is

$$\Delta t_{ii} \leq \frac{2}{\rho\left(\mathbf{R}_{ii}^{-1}\mathbf{S}_{ii}\right)} \quad \text{in conductor domain.} \tag{29}$$

Next, we compare the stability criteria for conductor and dielectric domains, and find out the smaller one to be used as the stability criterion of the entire system. The $\rho(\mathbf{R}_{ii}^{-1}\mathbf{S}_{ii})$ and $\rho(\mathbf{T}_{oo}^{-1}\mathbf{S}_{oo})$ are the largest eigenvalue that can be found from solving $\mathbf{S}_{ii}\{x\} = \lambda_i \mathbf{R}_{ii}\{x\}$, and $\mathbf{S}_{oo}\{x\} = \lambda_o \mathbf{T}_{oo}\{x\}$, respectively, in which λ_i and λ_o are eigenvalues. Considering the relationship between the magnitude of the matrix elements in $\mathbf{R}$ and that in $\mathbf{T}$, as shown in (16), we identify the following relationship between λ_i and λ_o:

$$\frac{\lambda_i}{\lambda_o} \sim \frac{\varepsilon_0 \varepsilon_r}{\sigma} \ll 1 \tag{30}$$

which means that $\rho(\mathbf{R}_{ii}^{-1}\mathbf{S}_{ii}) < \rho(\mathbf{T}_{oo}^{-1}\mathbf{S}_{oo})$. Even after taking a square root of $\rho(\mathbf{T}_{oo}^{-1}\mathbf{S}_{oo})$, Δt_{ii} is greater than Δt_{oo}. As a result, the stability criterion of the combined dielectric-conductor problem is governed by that of the dielectric domain.

IV. NUMERICAL RESULTS

We have simulated a number of examples to demonstrate the accuracy and efficiency of the proposed method. The computer used has an Intel Xeon CPU E5410 running at 2.33 GHz.

First, we assess the accuracy of the proposed direct solution of the Schur complement shown in (14). The example considered is a cube that is half filled by copper, the conductivity of which is 5.0 e + 7 S/m. The dimension of the cube is set based on typical on-chip circuit dimensions, as shown in Fig. 6. The mesh size is 1 μm, both inside and outside conductors in this example. The dielectric region is free space. The open boundary condition is employed to truncate the computational domain. The relative error between $\mathbf{A}_{ii}^{-1}$ and $[\mathbf{A}_{ii} - \mathbf{A}_{io}\mathbf{A}_{oo}^{-1}\mathbf{A}_{oi}]^{-1}$ is evaluated by

$$\mathrm{E}_{\mathrm{relative(direct)}} = \frac{\left\| \left[\mathbf{A}_{ii} - \mathbf{A}_{io}\mathbf{A}_{oo}^{-1}\mathbf{A}_{oi}\right]^{-1} - \mathbf{A}_{ii}^{-1} \right\|}{\left\| \left[\mathbf{A}_{ii} - \mathbf{A}_{io}\mathbf{A}_{oo}^{-1}\mathbf{A}_{oi}\right]^{-1} \right\|}. \tag{31}$$

In addition, as shown in Section III, if a higher order of accuracy is pursued, Neumann series (19) can be employed to solve (14) with a few terms. Its relative error as compared to $[\mathbf{A}_{ii} - \mathbf{A}_{io}\mathbf{A}_{oo}^{-1}\mathbf{A}_{oi}]^{-1}$ is evaluated by (32), shown at the bottom of the page, in which n denotes the number of terms in Neumann series. In fact, when $n = 1$, Neumann series (19) becomes $\mathbf{A}_{ii}^{-1}$, and hence the direct solution of (14) becomes the direct solution of (18). Table I shows the calculated relative error with respect to different time step Δt. As can be seen, the relative error is very small even with a very small Δt that is typically used in a conditionally stable explicit method for simulating on-chip circuits. When Δt increases, the relative error decreases. Therefore, for both conditionally stable schemes that have a small time step and unconditionally stable schemes that have a large time step, (18) constitutes an accurate solution of (14). Table I also shows the relative error with respect to the number of expansion terms in Neumann series. As can be seen, when the number of terms used in the Neumann series increases, the relative error decreases. Since the accuracy of the one-term Neumann series (i.e., using $\mathbf{A}_{ii}^{-1}$ only) is satisfactory, it is used in all the following examples.

The second example is a realistic test-chip interconnect structure of length 100 μm provided by Intel Corporation. This test-chip interconnect structure was fabricated using conventional silicon processing technology. It comprised three metal layers and 13 inhomogeneous dielectric stacks, which is illustrated in Fig. 7. The smallest mesh size inside conductors is 0.2 μm, while the mesh size outside conductors is 5 μm. A current source, which is a time derivative Gaussian pulse $I(t) = 2t\exp(-t^2/\tau^2)$ (τ = 3.0e-12 s), was placed at the near-end of the interconnect. The far end was left open, which

$$\mathrm{E}_{\mathrm{relative(Neumann},n\ \mathrm{terms})} = \frac{\left\| \left[\mathbf{A}_{ii} - \mathbf{A}_{io}\mathbf{A}_{oo}^{-1}\mathbf{A}_{oi}\right]^{-1} - \left(\sum_{k=1}^{n} \left[\mathbf{A}_{ii}^{-1}\left(\mathbf{A}_{io}\mathbf{A}_{oo}^{-1}\mathbf{A}_{oi}\right)\right]^{k-1}\right)\mathbf{A}_{ii}^{-1} \right\|}{\left\| \left[\mathbf{A}_{ii} - \mathbf{A}_{io}\mathbf{A}_{oo}^{-1}\mathbf{A}_{oi}\right]^{-1} \right\|} \tag{32}$$

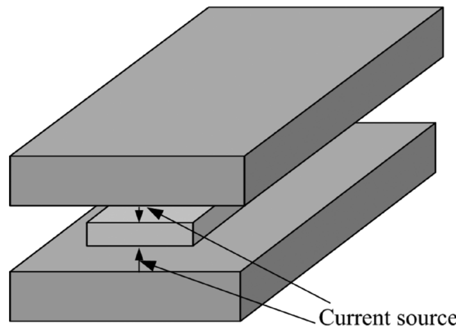

Fig. 7. Test-chip interconnect structure (provided by Intel Corporation).

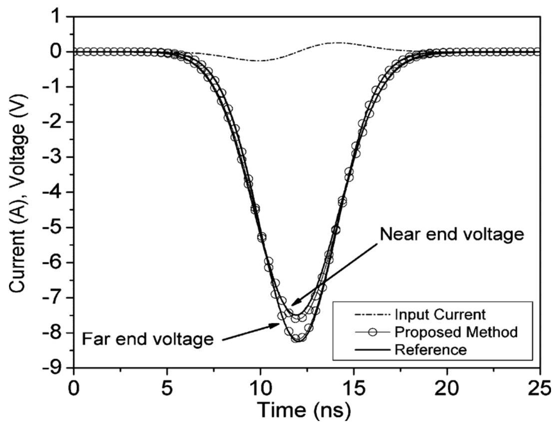

Fig. 8. Comparison of time-domain waveforms obtained by the proposed method and reference data provided by the OrFE-RR method [9] for a test-chip interconnect.

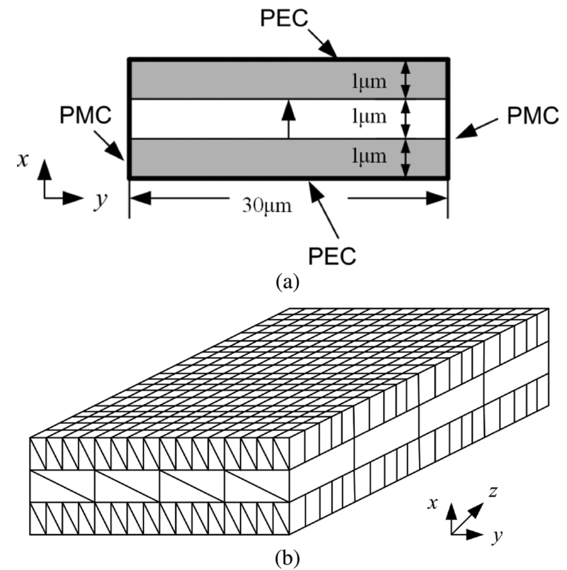

Fig. 9. (a) Geometry of a lossy parallel plate waveguide (PEC and PMC boundaries are shown by darker lines). (b) Discretization with nonconformal meshes.

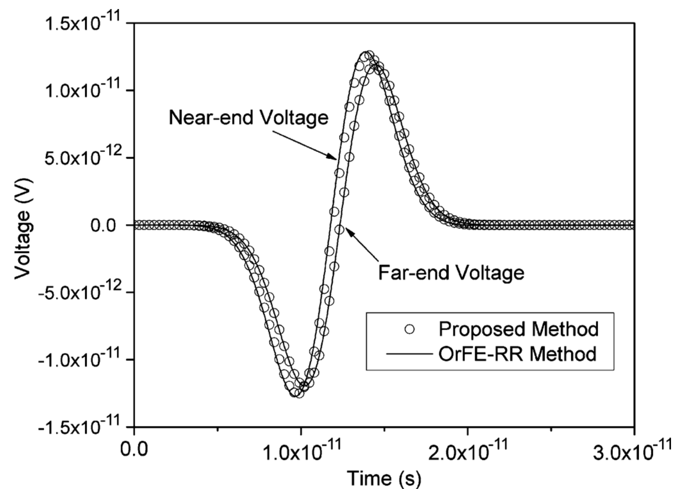

Fig. 10. Time-domain waveforms at the near-end and far-end of the lossy parallel plate waveguide.

is then truncated by the first-order absorbing boundary condition. The time step used in the simulation was 1.2e-16 s. In this example, we discretized the structure using a conformal mesh, in which the mesh in the conductor domain and that in the dielectric domain match at their interface. Fig. 8 shows the time-domain waveforms of the voltages sampled at the near-end and far-end of the center strip in the interconnect structure. Clearly, the result obtained by the proposed method is in excellent agreement with that obtained from the orthogonal finite-element reduction-recovery (OrFE-RR) method that was fully validated in [9].

To assess the capability of the proposed method in supporting a nonconformal mesh, we simulated a lossy parallel plate waveguide, the length of which was 100 μm. The height of the waveguide was 3 μm, and the width was 30 μm, as shown in Fig. 9(a). The smallest mesh size is 1 μm used inside conductors, while the largest size is 7.5 μm used outside conductors. The conductivity of the conductors was 5.0e+7 S/m. The dielectric material between the two conductors was air. The computational domain was truncated by a perfect electric conductor (PEC) boundary condition on the topmost surface and at the bottommost surface, a perfect magnetic conductor (PMC) boundary condition on the left and the right, and a first-order absorbing boundary condition in the front and at the back. The discretization was performed using a nonconformal mesh, as shown in Fig. 9(b). A fine mesh was used in the conductor domain, while a coarse mesh was used in the dielectric domain, resulting in 8287 unknowns. The mesh at the interface between the conductor domain and the dielectric domain did not match. A current source was launched at the near-end of the structure. In Fig. 10, we plot the time-domain waveforms obtained by the proposed method in comparison with those from the OrFE-RR method [9]. Excellent agreement is observed. In the OrFE-RR method, the discretization has to be done based on a conformal mesh. Restricted by the fine mesh required for discretizing the conductor region, the mesh in the dielectric region was much finer than necessary. The resultant number of unknowns was 10 831, which was larger than that generated by the proposed method. In this example, the dielectric region only occupied a small portion of the entire problem. The advantage of the proposed method in saving the number of unknowns will be even more obvious for problems having larger dielectric regions, like realistic VLSI circuits, in which the dielectric region usually occupies more than half of the entire computational domain. To demonstrate this fact, we simulated a lossy parallel plate waveguide of 10-μm height, 100-μm

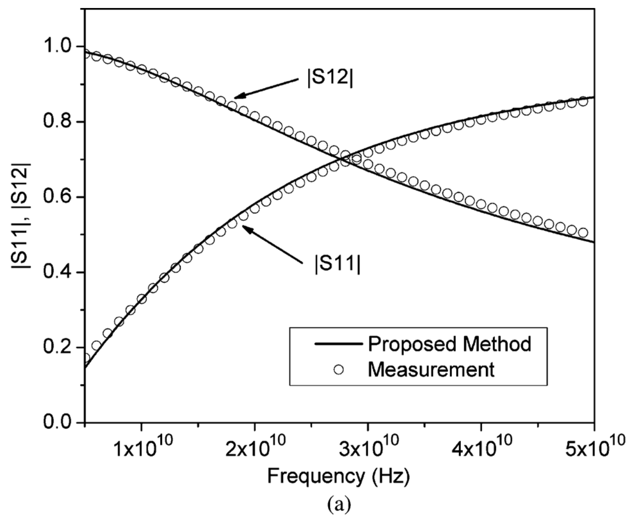

(a)

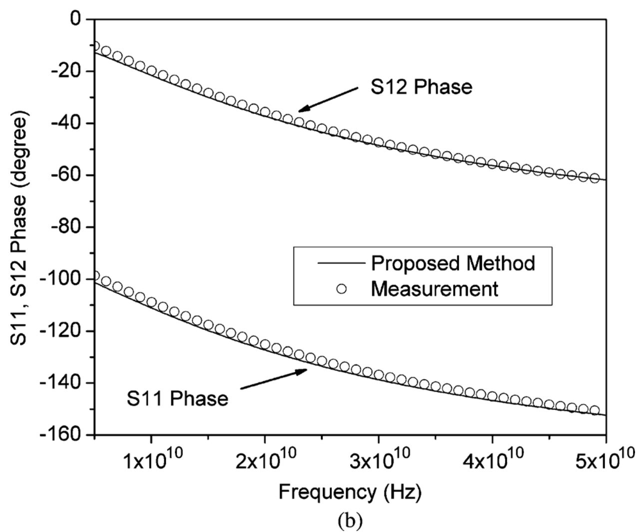

(b)

Fig. 11. (a) S11 and S12 magnitude versus frequency. (b) S11 and S12 phase versus frequency. (Measurements from [20].)

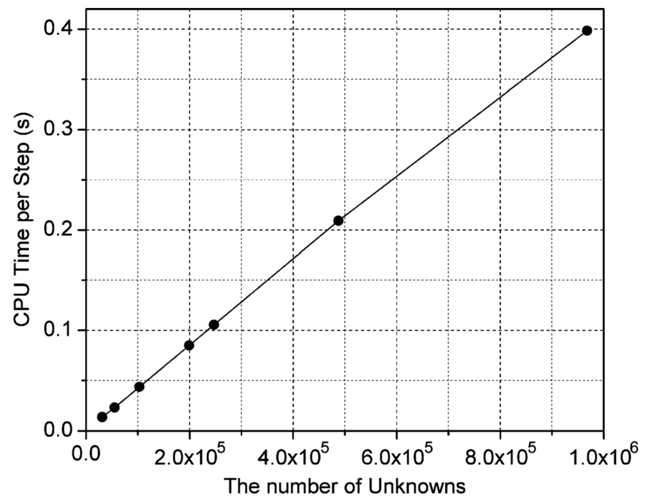

Fig. 12. CPU time per step versus the number of unknowns.

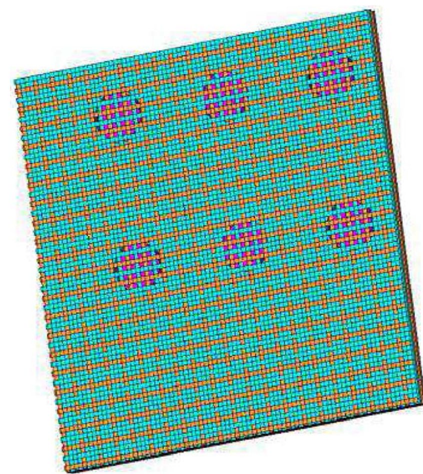

Fig. 13. Bottom view of the combined die-package structure.

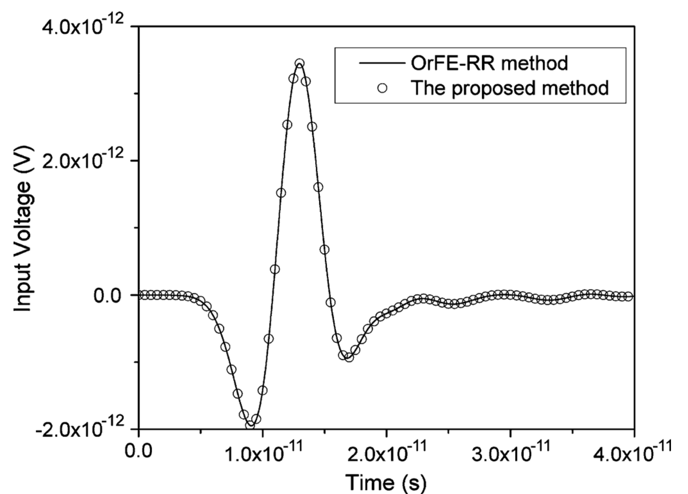

Fig. 14. The input voltage between a VSS (ground) via and the substrate.

width, and 2000-μm length. With the conformal mesh used in the OrFE-RR method, the number of unknowns was 1 031 210; with the nonconformal mesh supported by the proposed method, the resultant number of unknowns was only 243 493. It took the OrFE-RR method 0.37 s to simulate this example at each time step, whereas the proposed method only cost 0.13 s.

Next, we resimulated the test-chip interconnect structure shown in Fig. 7 based on a nonconformal mesh, and compared the results with the measured data provided by Intel Corporation. We kept the mesh inside the conductors the same as before but used a coarser mesh outside the conductors. Specifically, we reduced the mesh density in the dielectric domain by half. We extracted the frequency-domain S-parameters of the interconnect structure and compared them with the measured data. Excellent agreement with the measured data can be seen from Fig. 11.

With the accuracy, flexibility, and efficiency of the proposed method validated, next, we examined the computational complexity of the proposed method. We kept the mesh density to be the same; and enlarged the test-chip interconnect structure shown in Fig. 7 to obtain a wide range of unknowns. We then plotted the central processing unit (CPU) time cost at each time step of the proposed method versus the number of unknowns, which is shown in Fig. 12. A clear linear scaling is observed.

Last but not the least, we simulated a more complicated structure, which is a realistic 2500 $\times$ 2500-μm^2 combined

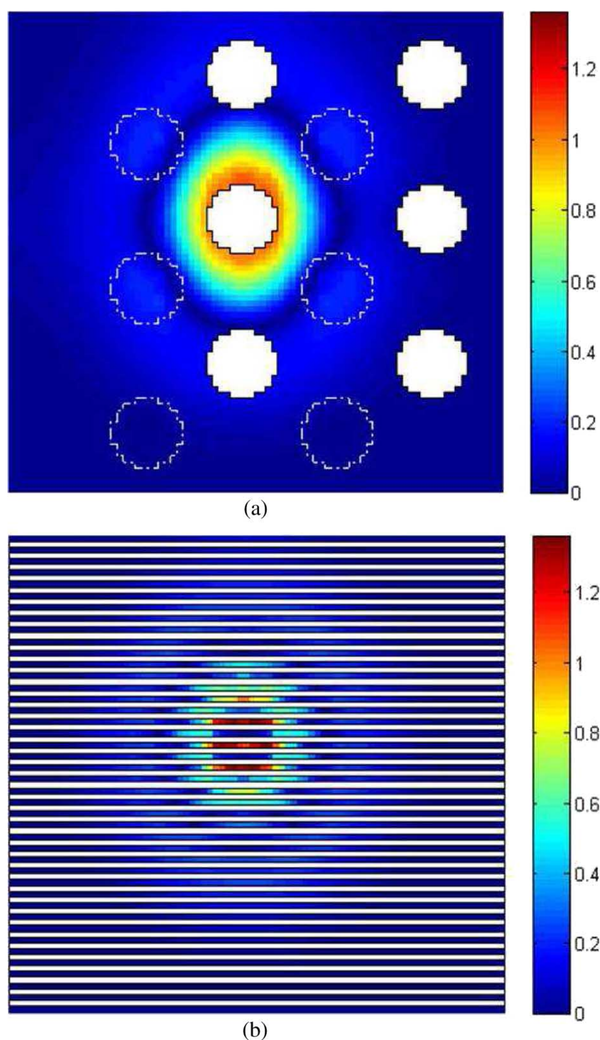

Fig. 15. Simulation of a 2500 $\times$ 2500-μm combined die-package system. (a) Voltage map of a package power plane. (b) Voltage map of one on-chip layer.

die-package power delivery system, provided by Intel Corporation. A real package structure was placed on top of the chip. The structure involved a bottom ground plane with via holes, a center via layer consisting of both power and ground vias, and a top power plane with via holes. A bottom ground via was excited by a current source. Three on-chip layers were at the bottom. Power and ground vias traversed via holes and contacted package planes. The on-chip power rails were connected through on-chip vias. An illustration of the structure is shown in Fig. 13. The mesh size used inside conductors is 0.5 μm, while the largest size outside conductors is 50 μm. A current source was launched at a ground via from the silicon substrate. The time step used in the simulation was 2.5e-14 s. The time-domain waveform of the input voltage excited by the current is plotted in Fig. 14. It shows excellent agreement with the results obtained from OrFE-RR solver. The voltage map of a power plane in the package and that of an on-chip layer at the 6000th time step were shown in Fig. 15.

V. Conclusion

In this paper, a direct domain-decomposition-based time-domain finite-element method of linear complexity is proposed to overcome the challenge of simulating a wide range of geometrical scales present in an IC system. The proposed method is capable of simulating lossy conductors with arbitrary shapes embedded in inhomogeneous dielectric materials. It permits the use of a nonconformal mesh, which makes the discretization much easier and meanwhile reduces the size of the problem. More important, the proposed method is a direct solver without any iteration, and it has linear complexity. The accuracy and efficiency of the proposed method have been demonstrated by realistic IC and package examples. The proposed method can be employed to perform the extraction of on-chip and package circuits, signal integrity, and power integrity analysis. It can also be applied to the electromagnetic analysis of other physical problems having lossy conductors and nonuniform dielectrics.

References

[1] M. Ha, K. Srinivasan, and M. Swaminathan, "Transient chip-package cosimulation of multiscale structures using the Laguerre-FDTD scheme," *IEEE Trans. Adv. Packag.*, vol. 32, no. 4, pp. 816–830, Nov. 2009.

[2] G. Antonini and A. E. Ruehli, "Waveform relaxation time domain solver for subsystem arrays," *IEEE Trans. Adv. Packag.*, vol. 33, no. 4, pp. 760–768, Nov. 2010.

[3] A. E. Yilmaz, J. M. Jin, and E. Michielssen, "A parallel FFT-accelerated transient field-circuit simulator," *IEEE Trans. Microw. Theory Tech.*, vol. 53, no. 9, pp. 2851–2865, Sep. 2005.

[4] J. E. Schutt-Aine, "Latency insertion method (LIM) for the fast transient simulation of large networks," *IEEE Trans. Circuits Syst. I, Fundam. Theory Appl.*, vol. 48, no. 1, pp. 81–89, Jan. 2001.

[5] R. Wang and J. M. Jin, "A symmetric electromagnetic-circuit simulator based on the extended time-domain finite element method," *IEEE Trans. Microw. Theory Tech.*, vol. 56, no. 12, pp. 2875–2884, Dec. 2008.

[6] V. Jandhyala, S. Chakroborty, D. Gope, C. Yang, I. Choudhury, and G. Ouyang, "Accelerated parallelized time and frequency domain simulation for complex high-speed microsystems," in *Proc. IEEE Antennas Propag. Soc. Int. Symp.*, Sep. 2006, pp. 123–126.

[7] H. Gan and D. Jiao, "Hierarchical finite element reduction recovery method for large-scale transient analysis of high-speed integrated circuits," *IEEE Trans. Adv. Packag.*, vol. 33, no. 1, pp. 276–284, Feb. 2010.

[8] H. Gan and D. Jiao, "A time-domain layered finite element reduction recovery (LAFE-RR) method for high-frequency VLSI design," *IEEE Trans. Antennas Propag.*, vol. 55, no. 12, pp. 3620–3629, Dec. 2007.

[9] D. Chen and D. Jiao, "Time-domain orthogonal finite-element reduction-recovery (OrFE-RR) method for electromagnetics-based analysis of large-scale integrated circuit and package problems," *IEEE Trans. Comput. Aided Design Integr. Circuits Syst.*, vol. 28, no. 8, pp. 1138–1149, Aug. 2009.

[10] H. Gan and D. Jiao, "An unconditionally stable time-domain finite element method of significantly reduced computational complexity for large-scale simulation of IC and package problems," in *Proc. IEEE 18th Conf. Electr. Performance Electron. Packag. Syst.*, 2009, pp. 145–148.

[11] S. C. Lee, M. N. Vouvakis, and J. F. Lee, "A non-overlapping domain decomposition method with non-matching grids for modeling large finite antenna arrays," *J. Comput. Phys.*, vol. 203, no. 1, pp. 1–21, Feb. 2005.

[12] H. Wu and A. C. Cangellaris, "A finite-element domain-decomposition methodology for electromagnetic modeling of multilayer high-speed interconnects," *IEEE Trans. Adv. Packag.*, vol. 31, no. 2, pp. 339–350, May 2008.

[13] S. H. Lee and J. M. Jin, "Efficient full-wave analysis of multilayer interconnection structures using a novel domain decomposition-model-order reduction method," *IEEE Trans. Microw. Theory Tech.*, vol. 56, no. 1, pp. 121–130, Jan. 2008.

[14] Z. Lou and J. M. Jin, "A novel dual-field time-domain finite-element domain-decomposition method for computational electromagnetics," *IEEE Trans. Antennas Propag.*, vol. 54, no. 6, pp. 1850–1862, Jun. 2006.

[15] K. Sun, Q. Zhou, K. Mohanram, and D. C. Sorensen, "Parallel domain decomposition for simulation of large-scale power grids," in *Proc. IEEE/ACM Int. Conf. Comput.-Aided Design*, 2007, pp. 54–59.

[16] R. Becker, P. Hansbo, and R. Stenberg, "A finite element method for domain decomposition with non-matching grids," *Math. Model. Numer. Anal.*, vol. 37, no. 2, pp. 209–225, 2003.

[17] F. Magoules, P. Ivanyi, and B. H. Vopping, "Convergence analysis of Schwarz methods without overlap for the Helmholtz equation," *Comput. Struct.*, vol. 82, no. 22, pp. 1835–1847, Sep. 2004.

[18] J. M. Jin, *The Finite Element Method in Electromagnetics*, 2nd ed. New York: Wiley, 2002.

[19] G. Meurant, "A review on the inverse of symmetric tridiagonal and block tridiagonal matrices," *SIAM J. Matrix Anal. Appl.*, vol. 13, no. 3, pp. 707–728, Jul. 1992.

[20] M. J. Kobrinsky, S. Chakravarty, D. Jiao, M. C. Harmes, S. List, and M. Mazumder, "Experimental validation of crosstalk simulations for on-chip interconnects using S-parameters," *IEEE Trans. Adv. Packag.*, vol. 28, no. 1, pp. 57–62, Feb. 2005.

[21] D. Jiao and J. M. Jin, "A general approach for the stability analysis of time-domain finite element method," *IEEE Trans. Antennas Propag.*, vol. 50, no. 11, pp. 1624–1632, Nov. 2002.

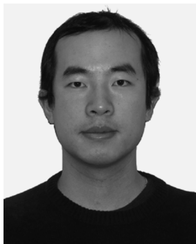

Duo Chen received the B.S. and M.S. degrees in electrical engineering from Tsinghua University, Beijing, China, in 2004, and 2007, respectively. Currently, he is working toward the Ph.D. degree in the School of Electrical and Computer Engineering, Purdue University, West Lafayette, IN.

He is a Research Assistant in the On-Chip Electromagnetics Research Group. His current research interest is electromagnetics-based analysis of very large scale integration (VLSI) and package problems.

Dan Jiao (S'00–M'02–SM'06) received the Ph.D. degree in electrical engineering from the University of Illinois at Urbana-Champaign, Urbana, in 2001.

She then worked at the Technology Computer-Aided Design (CAD) Division, Intel Corporation, until September 2005, as a Senior CAD Engineer, Staff Engineer, and Senior Staff Engineer. In September 2005, she joined Purdue University, West Lafayette, IN, as an Assistant Professor with the School of Electrical and Computer Engineering, where she is now a tenured Associate Professor. She has authored two book chapters and over 170 papers in refereed journals and international conferences. Her current research interests include computational electromagnetics; high-frequency digital, analog, mixed-signal, and RF integrated circuit (IC) design and analysis; high-performance very large scale integration (VLSI) computer-aided design (CAD); modeling of microscale and nanoscale circuits; applied electromagnetics, fast and high-capacity numerical methods; fast time-domain analysis; scattering and antenna analysis; RF; microwave; and millimeter-wave circuits; wireless communication; and bioelectromagnetics.

Dr. Jiao has served as the reviewer for many IEEE journals and conferences. She is an Associate Editor of the IEEE TRANSACTIONS ON COMPONENTS, PACKAGING, AND MANUFACTURING TECHNOLOGY. She was among the 85 engineers selected throughout the nation for the National Academy of Engineering's 2011 U.S. Frontiers of Engineering Symposium. She was the 2010 recipient of the Ruth and Joel Spira Outstanding Teaching Award; the 2008 National Science Foundation (NSF) CAREER Award; the 2006 Jack and Cathie Kozik Faculty Start up Award (which recognizes an outstanding new faculty member of the School of Electrical and Computer Engineering, Purdue University); a 2006 Office of Naval Research (ONR) Award under the Young Investigator Program; the 2004 Best Paper Award presented at the Intel Corporation's annual corporate-wide technology conference (Design and Test Technology Conference) for her work on generic broadband model of high-speed circuits; the 2003 Intel Corporation's Logic Technology Development (LTD) Divisional Achievement Award in recognition of her work on the industry-leading BroadSpice modeling/simulation capability for designing high-speed microprocessors, packages, and circuit boards; the Intel Corporation's Technology CAD Divisional Achievement Award for the development of innovative full-wave solvers for high frequency IC design, the 2002 Intel Corporation's Components Research the Intel Hero Award (Intel-wide she was the tenth recipient) for the timely and accurate 2-D and 3-D full-wave simulations; the Intel Corporation's LTD Team Quality Award for her outstanding contribution to the development of the measurement capability and simulation tools for high-frequency on-chip crosstalk; and the 2000 Raj Mittra Outstanding Research Award presented by the University of Illinois at Urbana-Champaign.